Electron energy-loss spectroscopy of boron-doped layers in amorphous thin film silicon solar cells

M. Duchamp, C. B. Boothroyd, M. S. Moreno, B. B. van Aken, W. J. Soppe, and R. E. Dunin-Borkowski

Citation: Journal of Applied Physics **113**, 093513 (2013); doi: 10.1063/1.4793587
View online: http://dx.doi.org/10.1063/1.4793587
View Table of Contents: http://scitation.aip.org/content/aip/journal/jap/113/9?ver=pdfcov
Published by the AIP Publishing

Electron energy-loss spectroscopy of boron-doped layers in amorphous thin film silicon solar cells

M. Duchamp,[1,a)] C. B. Boothroyd,[1] M. S. Moreno,[2] B. B. van Aken,[3] W. J. Soppe,[3] and R. E. Dunin-Borkowski[1]
[1]*Ernst Ruska-Centre for Microscopy and Spectroscopy with Electrons (ER-C) and Peter Grünberg Institute (PGI), Forschungszentrum Jülich, D-52425 Jülich, Germany*
[2]*Centro Atómico Bariloche, 8400 - S. C. de Bariloche, Argentina*
[3]*ECN Solar Energy, High Tech Campus, Building 5, 5656 AE Eindhoven, The Netherlands*

(Received 10 December 2012; accepted 12 February 2013; published online 7 March 2013)

Electron energy-loss spectroscopy (EELS) is used to study *p*-doped layers in *n-i-p* amorphous thin film Si solar cells grown on steel foil substrates. For a solar cell in which an intrinsic amorphous hydrogenated Si (*a*-Si-H) layer is sandwiched between 10-nm-thick *n*-doped and *p*-doped *a*-Si:H layers, we assess whether core-loss EELS can be used to quantify the B concentration. We compare the shape of the measured B K edge with real space *ab initio* multiple scattering calculations and show that it is possible to separate the weak B K edge peak from the much stronger Si L edge fine structure by using log-normal fitting functions. The measured B concentration is compared with values obtained from secondary ion mass spectrometry, as well as with EELS results obtained from test samples that contain ~200-nm-thick *a*-Si:H layers co-doped with B and C. We also assess whether changes in volume plasmon energy can be related to the B concentration and/or to the density of the material and whether variations of the volume plasmon line-width can be correlated with differences in the scattering of valence electrons in differently doped *a*-Si:H layers. © *2013 American Institute of Physics*. [http://dx.doi.org/10.1063/1.4793587]

INTRODUCTION

The roll-to-roll production of *n-i-p* thin film Si solar cells is a promising way to achieve large volume production of cheap and efficient devices on lightweight, flexible supports, since the layers can be deposited directly onto opaque substrates at low temperature. Both amorphous (*a*-Si:H) and microcrystalline (μc-Si:H) hydrogenated Si solar cells are currently grown on glass, plastic, and steel foil substrates, both in the laboratory and on industrial scales.[1] For *n-i-p* solar cells, the Si deposition sequence starts from *n*-doped Si, followed by the intrinsic (*i*) and *p*-doped Si layers. The i-Si:H layer is therefore sandwiched between ~10-nm-thick *n*- and *p*-doped *a*-Si:H layers, which need to satisfy the two opposing requirements of high conductivity and low carrier recombination rate. In addition, the *p*-doped layer should be as transparent as possible to reduce parasitic optical absorption. One approach that can be used to increase its transparency is to alloy it with C to increase its optical band gap.[2] It is also important to confine the dopant to the *p* layer to limit B contamination of the *i*-Si layer, which degrades the carrier mobility[3] and the local atomic order[4] and weakens the strength of the electric field in the *i*-layer near the *p*/*i* interface resulting in a lower carrier collection efficiency.[5] On flat thin film Si solar cells, Kroll *et al*. showed a clear correlation between degradation of solar cell performance and B contamination of the *i*-Si:H layer by using secondary ion mass spectrometry (SIMS).[5] The impact of boron-oxygen-related recombination centres has been studied extensively for B-doped Czochralski-grown Si,[6] as they ultimately limit the carrier lifetime.[7] For all of these reasons, it is important to be able to measure the B concentration in *p*- and *i*-doped *a*-Si:H layers with nanometre spatial resolution and to correlate these measurements with solar cell performance.

Our preliminary measurements of B concentration using core-loss electron energy-loss spectroscopy (EELS) in the transmission electron microscope (TEM), which are reported elsewhere,[8] required the use of a long acquisition time to detect low B concentrations in *a*-Si:C:H and *a*-Si:H layers and careful analysis to extract the B K edge from the Si $L_{2,3}$ fine structure. Other attempts in the literature to measure low B concentrations using EELS have reported detection limits for B of 0.2% with 10% accuracy in B-doped C,[9] 0.5% in Ni_3Al (Ref. 10), and 1% in Si (Ref. 11). In a recent study, Asayama *et al*. managed to detect 0.2.% B in a *p*-type Si device using a spherical aberration corrected scanning TEM (STEM).[12] The difficulty of such measurements results in part from the fact that the energy-loss near-edge structure (ELNES) from the Si L edge, caused by scattering of inner-shell electrons to the conduction band, extends from 99 to 300 eV and interferes with the B K edge at 188 eV. In addition, the Si $L_{2,3}$ edge cross-section is five times larger than that of the B K edge. When combined with the fact that the B concentration is only a few percent, the Si peak intensity is hundreds of times larger than that of the B K edge.

In addition to measurements of B concentration, it is equally important to determine the proportion of B atoms that is electrically active in the *p*-doped layer in an *a*-Si:H solar cell. In the free electron model, the volume plasmon energy is proportional to the square root of the valence electron density, while the line-width of the plasmon resonance

a)Author to whom correspondence should be addressed. Electronic mail: m.duchamp@fz-juelich.de. Tel.: +49 2461 61 9478.

is inversely proportional to the relaxation time of the plasmon oscillation.[13] For high B concentrations (up to 24%), a volume plasmon energy shift of 0.8 eV has been measured using X-ray photoelectron spectroscopy.[4]

In the first part of this paper, we describe the growth of our *a*-Si:H layers using plasma-enhanced chemical vapour deposition (PECVD). We then present a detailed explanation of the methodology that we use to determine the B concentration with core-loss EELS. Our measured B concentrations are compared with SIMS measurements from the same samples. In the third part of the paper, variations in volume plasmon energy across the doped layers are measured and discussed with reference to their local chemical and electrical properties.

EXPERIMENTAL DETAILS

Layer deposition was carried out in a Flexicoat300 industrial pilot roll-to-roll system, which is used for PECVD growth of doped and intrinsic Si layers on steel foils that have widths of up to 300 mm using three in-line deposition chambers (Fig. 1). Two of the chambers are equipped with linear symmetric RF (13.56 MHz) sources[14] that are suitable for the deposition of amorphous or micro-crystalline doped Si layers. The intrinsic Si:H absorber layers are deposited using a linear very high frequency (VHF) plasma source (70 MHz). The use of different chambers to deposit the differently-doped layers minimises possible cross-contamination and subsequent contamination of the intrinsic layer. Test samples ($10 \times 2.5\,cm^2$ in size) were fixed onto a custom-made sample holder, which was placed on the steel foil. Real solar cell samples were grown directly on steel foil.

Samples were prepared for TEM observation using a standard lift-out procedure in a dual-beam FEI Helios focused ion beam (FIB) workstation. ~200 nm of electron-beam-deposited Pt and ~1 μm of ion-beam-deposited Pt were used to avoid degradation of the samples due to Ga^{2+} implantation. Coarse FIB milling was carried out using a 30 kV ion beam, while final milling was performed using a 1 kV ion beam. Each sample was cleaned at 500 V using a focused Ar beam in a Fischione Nanomill system to remove the Ga-contaminated surface layer.

Core-loss EEL spectra were acquired in TEM diffraction mode (image coupling to the spectrometer) at 120 kV in an FEI Tecnai microscope. We chose a collection semi-angle of 10 mrad using an objective aperture and a low camera length to maximise the signal when using a 2 mm Gatan imaging filter (GIF) entrance aperture, while maintaining a reasonable signal-to-noise ratio. For core-loss measurements, the nanobeam mode of the microscope and a small condenser aperture were used to form a 50 nm parallel electron beam for the test samples and to reduce the beam diameter to ~3 nm for measurements from the *p*-doped layer in the real solar cell. For long acquisition times (with a high number of counts), channel-to-channel gain variation in the GIF camera is the dominant source of artefacts in the recorded spectra. We therefore used an iterative averaging procedure, which is described in detail elsewhere,[10] to reduce channel-to-channel gain variation. The sample thickness was measured by applying the "log-ratio method" to the low-loss EELS intensity and found to be ~80 nm. In order to check for the effect of plural scattering, the Si ELNES from the ~80-nm-thick sample was compared after Fourier deconvolution and with measurements obtained from a ~20-nm-thick sample. Apart from a small difference arising from the contribution of the volume plasmon peak due to plural scattering, the same peaks were present in the ELNES in each case. As the contribution from the volume plasmon peak was small and in order to avoid introducing additional noise in the spectra due to deconvolution, all of the results presented below were obtained from ~80-nm-thick TEM lamellae without performing any deconvolution.

Low-loss EEL spectra were acquired at 120 kV in STEM mode using a dispersion of 0.02 eV/pixel, while simultaneously collecting high-angle angular-dark-field (HAADF) images in an FEI Titan probe-corrected TEM. The typical acquisition time was ~1 s for each spectrum and the total number of spectra was ~500. Sample drift during acquisition was taken into account by using cross-correlation of images acquired every five spectra. The collection semi-angle of 10 mrad was defined by the objective aperture. The cut-off angle for scattering from volume plasmons in Si is 6.5 mrad (for higher angles, plasmons become highly damped as they can transfer all of their energy to single electrons by the creation of electron-hole pairs[13]). A 10 mrad collection angle is therefore small enough to avoid too large a contribution to the spectrum from single electron excitations, although contributions from different scattering angles will cause a slight broadening of the plasmon peak and a shift in its energy when compared to the plasmon peak energy expected for completely free electrons.

A scanning electron microscope (SEM) image of a typical cross-sectional FIB-prepared solar cell is shown in Fig. 2(a). The layer sequence in the growth direction is: Ag back contact, B-doped ZnO, *n*-doped *a*-Si:H, intrinsic *a*-Si:H, B- and C-co-doped *a*-Si:H, indium tin oxide (ITO) front

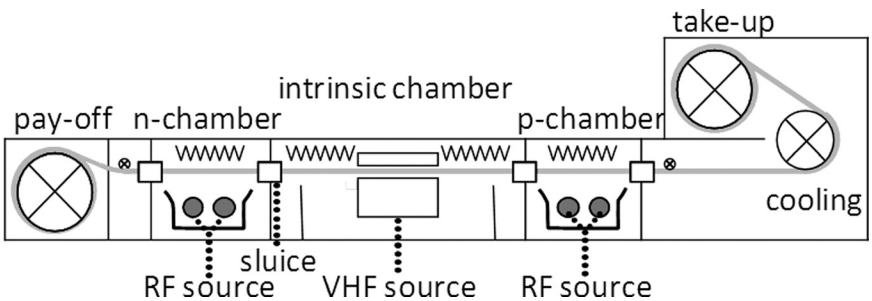

FIG. 1. Schematic diagram of the PECVD roll-to-roll deposition chambers used to grow thin film Si solar cells on metallic foil. Each chamber is dedicated to the deposition of a particular Si layer. From left to right, P-doped, undoped, and B- and C-co-doped Si layers.

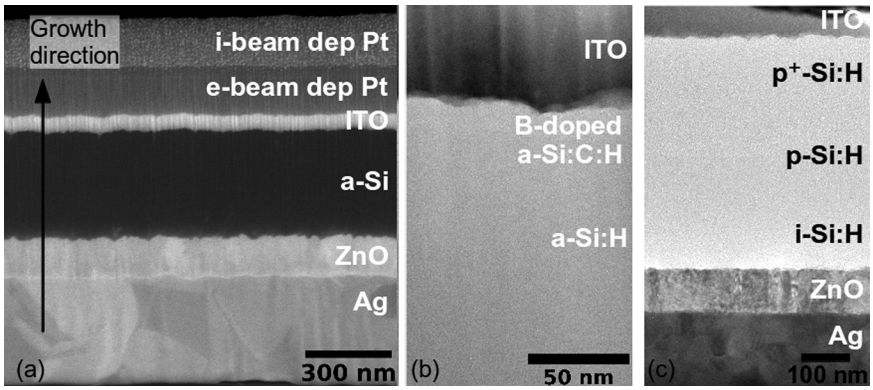

FIG. 2. (a) Secondary electron SEM image of a FIB-prepared cross-sectional TEM sample of a solar cell. From the bottom to the top: Ag back contact reflector deposited on steel substrate (not shown), ZnO, *a*-Si:H, ITO, e-beam, and i-beam deposited Pt. (b) Bright-field TEM image of the B-doped *a*-Si:C:H (*p*)/ITO interface in the solar cell sample shown in (a). (c) Bright-field TEM image of *a*-Si:H test sample 1.

contact. The C concentration in the top layer is expected to be ~20 at. %. We refer to this layer as *p*-doped *a*-Si:C:H. A bright-field (BF) TEM image of the *p*-doped *a*-Si:C:H layer, which is studied in detail below, is shown in Fig. 2(b). The *a*-Si:H and *p*-doped *a*-Si:C:H regions have similar BF contrast and cannot be distinguished from each other in Fig. 2(b). The total Si layer thickness is ~400 nm while the expected thickness of the *p*-doped *a*-Si:C:H layer is ~15 nm. The ~5 nm roughness of the *p*-doped *a*-Si:C:H/ITO interface reduces the depth resolution of SIMS measurements of the B concentration. For such a thin layer, a TEM beam diameter that is smaller than the layer thickness must be used, while optimizing the beam current density and acquisition time to limit irradiation damage. Due to these limitations, two additional test samples were prepared to provide complementary EELS measurements. The layer structure in test sample 1 (Fig. 2(c)) is: *a*-Si:H (i), *p*-doped *a*-Si:H with a B concentration similar to that of the *p*-doped layer in the solar cell (*p*) and *a*-Si:H deposited using twice the diborane concentration (p^+). Test sample 2 is identical to test sample 1, but all of the Si layers are alloyed with C in the same proportion as in the *p*-doped layer in the real solar cell. The thickness of each layer in the test samples is ~200 nm.

MEASUREMENT OF B CONCENTRATION USING CORE-LOSS EELS

Background-substracted EEL spectra recorded at the position of the Si $L_{2,3}$ edge from the three layers with different B concentrations (undoped, lightly doped, and highly doped) in the two test samples (*a*-Si:C:H and a *a*-Si:H) are shown in Fig. 3. The shoulder at 284 eV is attributed to the C K edge for the *a*-Si:C:H sample and is not observed for the *a*-Si:H sample. Elemental Si and C concentrations were determined from the spectra by subtracting the background from the Si $L_{2,3}$ and C K pre-edge regions using standard inverse power laws and integrating the resulting signals over an energy range between 5 and 20 eV beyond the edge onset. Cross-sections were determined using the Hartree-Slater model[15] and are given in Table I. Although the measured concentrations should be independent of the width of the integration window, variations result from errors in background subtraction and in the calculated cross-sections. An average of the C concentrations measured using different integration windows provides a value of 15.2% ± 1% for the *a*-Si:C:H layers (Table I).

The B K edge has a much smaller cross-section than the Si L edge (see Table I) and lies on an oscillating background arising from the fine structure of the Si $L_{2,3}$ and L_1 edges, making it difficult to determine the origin of the peaks observed in this energy range. In the present study, interpretation of the recorded spectra was facilitated by comparing results obtained from differently doped specimens and by removing the background under the B K edge in stages. First, the contribution of the structure of the Si $L_{2,3}$ edge to the background below the Si L_1 edge was removed from the background-substracted Si $L_{2,3}$ edge spectra by using a log-normal function of the form:

$$f(E,\sigma) = \frac{A}{(E-E_0)\sigma}\exp - \frac{(\log(E-E_0))^2}{2\sigma^2}, \qquad (1)$$

where E is energy loss and the constants A, σ, E_0 are fitted over a chosen energy range using a least-squares fitting method implemented in Gnuplot software.[16] A similar

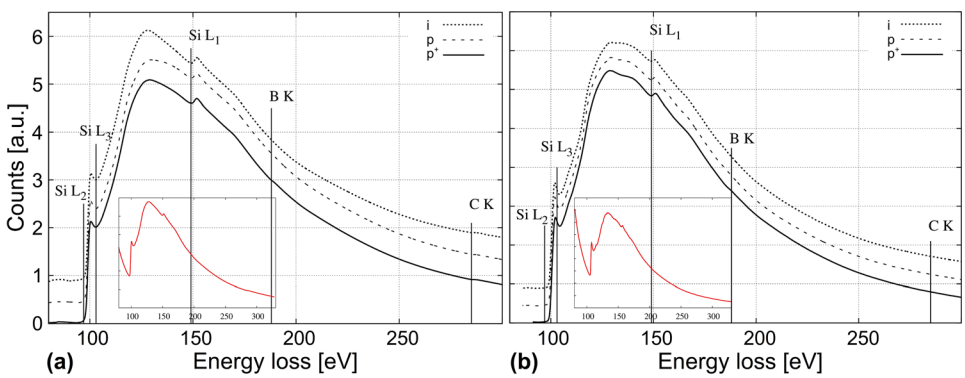

FIG. 3. Background-subtracted EEL spectra acquired near the Si $L_{2,3}$ edge for three different B concentrations labelled *i*, *p*, and p^+ in the (a) *a*-Si:C:H and (b) *a*-Si:H test samples. The spectra have been offset from each other vertically for clarity. The corresponding B concentrations measured using SIMS are given in Table I. The original spectra from the highly B-doped layers before background subtraction are shown as insets.

TABLE I. B and C atomic concentrations measured using core-low EELS from the *a*-Si:H and *a*-Si:C:H test samples. The hydrogen concentration is not taken into account for the calculation of the atomic concentrations. The concentrations measured using SIMS assume an atomic density of 5×10^{22} cm^{-3}. Cross-sections are calculated using the Hartree-Slater model (Ref. 15). Calculation errors in cross-sections are estimated to be ~20% (Ref. 2).

		Calculated cross-section (Barns)		Si:C:H			Si:H		
	Integration window (eV)	B or C	Si	*i*	*p*	p^+	*i*	*P*	p^+
C (at. %)	10	898	15 869	14.22	15.34	16.35	…	…	…
	20	1669	32 837	13.73	17.29	14.25	…	…	…
B (at. %)	5	1242	6881	0	1.75	3.57	0	1.19	3.87
	10	2333	15 869	0	1.12	6	0	1.05	4.96
	20	4209	32 837	0	0.5	5.24	0	0.49	2.55
	Average	…	…	0	1.1 ± 0.5	4.9 ± 1	0	0.9 ± 0.3	3.8 ± 1
	B (at. %) measured using SIMS			$3 \cdot 10^{-3}$	0.6	3.04	$3 \cdot 10^{-3}$	1.4	6

approach was used by Poe *et al*. to remove contributions to the atomic continuum after the Si K and $L_{2,3}$ edges to examine mixed Si coordination compounds varying in Si^{VI}:Si^{IV} ratios.[17] The resulting background-substracted Si L_1 edge spectra are shown in Fig. 4 for the two test samples. The effect of the presence of C on the local structure of the amorphous material can be seen in the form of differences between Figs. 4(a) and 4(b), which result from the different atomic coordinations and interatomic distances of Si atoms when they are surrounded by C instead of Si. The Si-Si and Si-C bond lengths have been computed and measured experimentally for *a*-SiC:H compounds to be 0.23 and 0.19 nm, respectively.[18] The B K edge at 188 eV is now more visible for the two highly doped (p^+) layers. For the lightly doped (*p*) samples, the B K edge is not as clearly visible on the Si L_1 edge fine structure.

In order to complete the separation of the B K edge from the Si fine structure, a conventional power law background subtraction was performed on the spectra shown in Fig. 4 and both the B K edge and the remaining Si fine structure at ~225 eV were fitted to log-normal functions (Eq. (1)). Figure 5 shows the best-fitting functions overlaid on the experimental spectra and compared with the results of real-space *ab initio* calculations of the B K edge performed using FEFF9 9.05 code[19] for the experimental values of acceleration voltage and collection angle. The calculation was performed for 5 at. % B in a disordered cluster, with core hole effects included by using the random phase approximation and the Hedin-Lundqvist self-energy to take inelastic losses into account. A reasonable match is obtained between the fitted and calculated B K edge shapes, although the fitted log-normal function has a slightly larger width. The concentration of B relative to that of Si was estimated from the areas under the log-normal functions for 5, 10, and 20 eV energy windows from the onset of the B K edges at 188 eV, making use of the Hartree-Slater cross sections[15] given in Table I. The observed variation in B concentration with energy window size is likely to result primarily from differences between the calculated and fitted edge shape, from the use of simple log-normal fitting functions that do not take the fine structure of the edge into account and from errors in background subtraction. In the present study, we simply averaged the results obtained using the different energy window sizes to determine final values for the measured B concentrations of 4.9 ± 1% and 3.8 ± 1% for the highly doped *a*-Si:C:H and *a*-Si:H layers and 1.1 ± 0.5% and 0.9 ± 0.3% for the lightly doped *a*-Si:C:H and *a*-Si:H layers, respectively (Table I). These values are within a factor of two of the SIMS measurements, which are also given in Table I. For the highest B concentrations (>1 at. %), the discrepancy between the two measurement techniques may be explained by matrix effects when high concentrations are measured using SIMS.[20]

The same procedure was used to measure the B concentration across the *p*-doped layer of the real solar cell from a linescan of EEL spectra acquired using 3 nm probe and step sizes. Figure 6 shows individual spectra after background subtraction of the Si $L_{2,3}$ edge. The C K edge is visible in the C-rich *p*-doped layer. At the same time, a variation in the fine structure of the Si L_1 edge is visible before the onset of

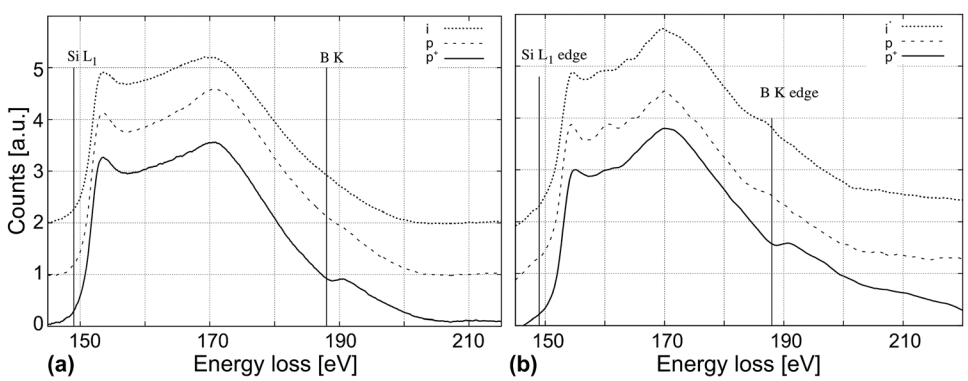

FIG. 4. Background-subtracted EEL spectra acquired near the Si L_1 edge for three different B concentrations labelled *i*, *p*, and p^+ in the (a) *a*-Si:C:H and (b) *a*-Si:H test samples. The spectra have been offset from each other vertically for clarity. The corresponding B concentrations measured using SIMS are given in Table I.

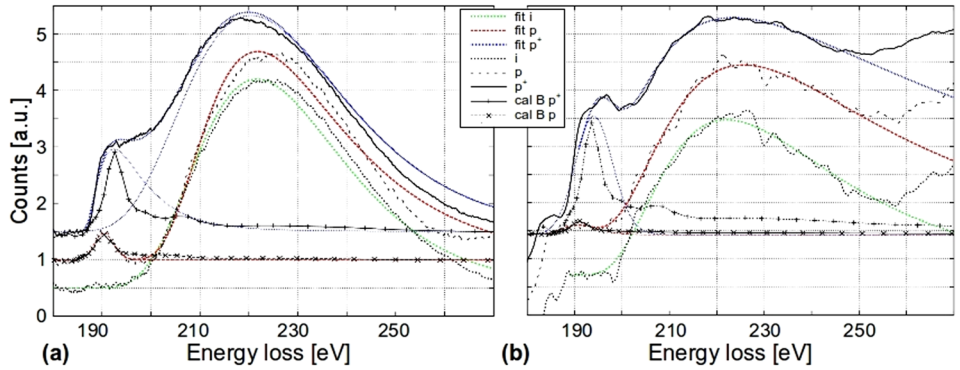

FIG. 5. Black lines: Background-subtracted EEL spectra acquired near the B K edge for three different B concentrations labelled *i*, *p*, and p^+ in the (a) *a*-Si:C:H and (b) *a*-Si:H test samples. Coloured dotted lines: Log-normal fits of the EXELFS peak centred at ~225 eV and of the B K edge. Different colours correspond to different B concentrations. Black lines with crosses: calculated B K edge for two different B concentrations. The corresponding B concentrations measured using SIMS are given in Table I. The spectra have been offset from each other vertically for clarity.

the B K edge. The relative B concentration was extracted from Fig. 6 using a 5 eV energy window and is plotted in Fig. 7 alongside SIMS measurements obtained using two different ion energies. (The best depth resolution is obtained using the lower ion energy at the expense of increased acquisition time). The shaded areas show the interfaces between the ITO and the *p*-doped *a*-Si:C:H layers on the left side and between the *p*-doped *a*-Si:C:H and *a*-Si:H layers on the right side. Further details about the sources of error for SIMS and core-loss EELS quantification are discussed elsewhere.[2] The results suggest that it is possible to use core-loss EELS to measure the concentration of B in the *p*-doped layer in real solar cells for a concentration of ~1 at. % with a spatial resolution of ~4 nm.

CHARACTERIZATION OF *p*-DOPED *a*-SI:H USING VOLUME PLASMON MEASUREMENTS

The position and the width of the volume plasmon peak depends on the local chemical and electrical properties of a material. Here, we assess whether variations in plasmon energy with B concentration can be measured in the two test samples. The energy dependence of the inelastically scattered intensity is proportional to $\Im[-1/\varepsilon(E)]$, where ε is the dielectric function and can be approximated, in the free-electron model,[12] by the expression

$$\Im\left[\frac{-1}{\varepsilon(E)}\right] = \frac{E_p^2(E\hbar/\tau)}{(E^2 - E_p^2)^2 + (E\hbar/\tau)^2}, \tag{2}$$

where E_p is the plasmon energy and τ is the plasmon relaxation time. The full width at half maximum of this function is given by $\Delta E_p = \hbar/\tau$. In the free electron model, the valence electron density (n) is related to the volume plasmon energy by

$$E_p = \hbar\sqrt{\frac{ne^2}{\varepsilon_0 m_0}}, \tag{3}$$

where $\hbar$, e, ε_0, and m_0 are the reduced Planck constant, electron charge, permittivity of free space and electron mass, respectively. In order to determine values for E_p and τ, we

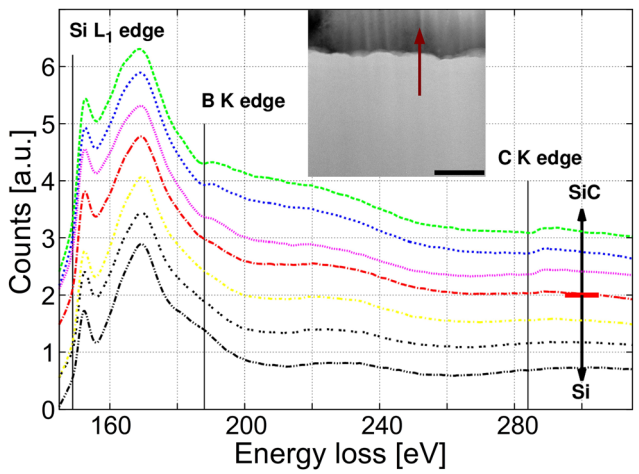

FIG. 6. Background-subtracted EEL spectra acquired near the Si L_1 edge at different positions on the sample near the *a*-Si:H/*p*-doped *a*-Si:C:H interface for the real solar cell sample. The red arrow indicates where the linescan was acquired in the bright-field TEM image shown as an inset. The scale bar in the bright-field TEM image is 50 nm.

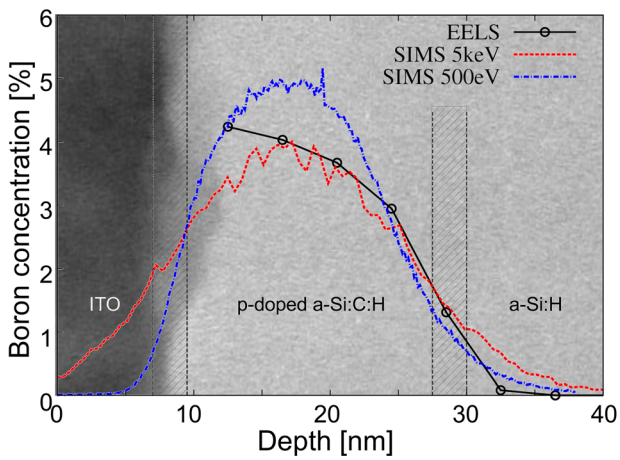

FIG. 7. Boron concentration in the *p*-doped *a*-Si:C:H layer in the real solar cell measured using core-loss EELS and SIMS. The B concentrations determined using core-loss EELS are extracted from the spectra shown in Fig. 6. The bright-field TEM image in the background shows the ITO/*p*-doped *a*-Si:C:H/*a*-SiH layer sequence from which EELS linescan was recorded.

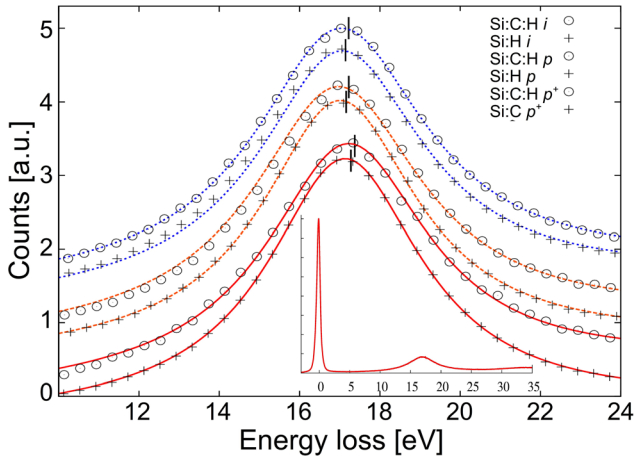

FIG. 8. Volume plasmon peaks measured from the *a*-Si:H and *a*-Si:C:H test samples doped with different B concentrations (see Table I). The small black vertical lines indicate the plasmon peak energies determined using Eq. (3), which lie slightly to the right of each peak maximum. The data points are measured values, while the continuous lines are fitted curves. For clarity, the plots are offset from each other vertically. A typical original spectrum, showing zero-loss and plasmon peaks, is shown in the inset.

fitted volume plasmon peaks measured using EELS to the function

$$I_{EELS}(E) = \frac{aE}{(E^2 - E_p^2)^2 + (E\Delta E_p)^2} + bE + c, \qquad (4)$$

in which the last two terms are included to take into account the unknown background contribution to the EELS signal, using a least-squares fitting method implemented in Gnuplot software.[16] For each recorded spectrum, the fits were used to obtain values for E_p and ΔE_p, as well as the fitting error in each parameter. In order to determine as precise a measurement of E_p as possible, the zero-loss peak (ZLP) was always recorded in the same spectrum as the volume plasmon peak and its position was determined by fitting a Lorentzian function to it. The values of E_p and ΔE_p were typically obtained with precisions of ~0.1%. Examples of volume plasmon spectra measured from the two test samples are shown in Fig. 8 for different B and C concentrations, with experimental data points shown using symbols (only one point out of ten is shown for clarity). The plasmon energies obtained by fitting each spectrum to Eq. (4) are indicated by vertical black lines and are slightly higher in energy than the maximum peak positions, in agreement with theory (Eq. (4)).

Plots of measured plasmon energy and peak width derived from linescans of spectra acquired across the p^+, *p*, and *i* layers in the Si:C:H and Si:H test specimens are shown in Fig. 9, alongside SIMS profiles measured from the same layers. The similarity between the plots is remarkable, especially the correlation between the decrease in the B concentration and the plasmon energy in the p^+ layers. Slight differences are measured at the *p*/*i* and *i*/contact layer interfaces which may be related to charge accumulation. The measured plasmon energies are ~17.3, ~17.23, and ~17.2 eV for the p^+, *p*, and *i* Si:C:H layers (Fig. 9(a)) and ~17.25, ~17.13, and ~17.1 eV for the p^+, *p*, and *i* Si:H layers (Fig. 9(b)), respectively. All of the experimental values are higher than that reported for crystalline Si (16.5 eV). This difference may have resulted from contributions to the spectra from different scattering vectors in the 10 mrad collection angle, or from the fact that H atoms have a lower ionization energy (1312 kJ mol^{-1}) than Si (786 to 4355 kJ mol^{-1} for the 4 outer shell electrons), such that electrons provided by H atoms can contribute to the valence electron cloud. These effects are partly compensated by the decrease in atomic density of *a*-Si:H by ~0.827 compared to that of crystalline Si.[21]

On the assumption that the volume plasmon energy varies linearly with doping concentration C_x in the form[22]

$$E_p(C_x) = E_p(0) + C_x \frac{dE_p}{dC_x}. \qquad (5)$$

Table II gives average values of dE_p/dC_x measured from the experimental data points shown in Fig. 9 for different B concentrations in the *a*-Si:H and *a*-Si:C:H samples. The variation in plasmon energy with B concentration is likely to result from a variation in (i) atomic density (B and Si have different covalent radii), (ii) electron density (B and Si have

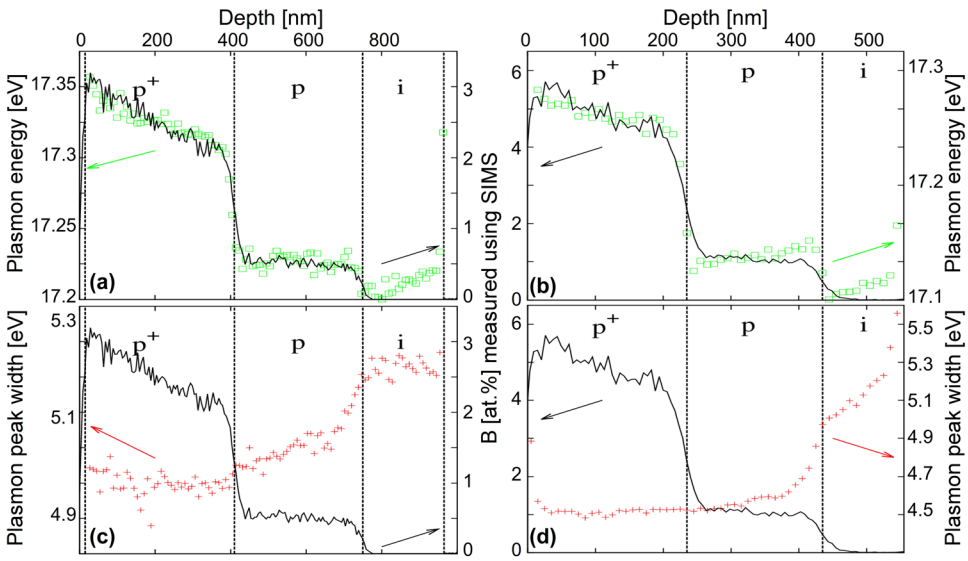

FIG. 9. (a,b) Plasmon peak energy and (c,d) peak width measured across the *i*, *p* and p^+ layers of the (a,c) *a*-Si:C:H and (b,d) *a*-Si:H test samples. The transitions between the differently-doped layers are shown using vertical dashed lines. The black lines show the B doping profiles measured using SIMS.

TABLE II. Parameters measured from volume plasmon spectra from the *i*, *p*, and p^+ layers of the *a*-Si:C:H and *a*-Si:H test samples (see text for details). E_p is the average plasmon peak energy (Fig. 8) and dE_p/dC is the change in average plasmon energy with B concentration. For each layer, $C_{B\text{-}EELS}$ and $C_{B\text{-}SIMS}$ are the average concentrations measured using EELS and SIMS, respectively (see Table I) and $C_{B\text{-}calc}$ is calculated using Eq. (6).

Compound	$dE_p/dC_{B\text{-}EELS}$ (eV)	$dE_p/dC_{B\text{-}SIMS}$ (eV)	$dE_p/dC_{B\text{-}calc}$ (eV)
a-Si:C:H	2.3 ± 0.3	4.1 ± 0.3	4
a-Si:H	3.5 ± 0.2	2.1 ± 0.2	4.6

different numbers of valence electrons), (iii) effective electron mass, and/or (iv) hydrogen concentration between the layers. For plasmon oscillations, the electron mass in vacuum typically provides reasonably accurate values of plasmon energy for many solids,[13] suggesting that variations in effective electron mass with B concentration may be neglected. Assuming for the moment that there is no significant change in hydrogen concentration, the effects of changes in valence and density can be considered in the form

$$\frac{dE_p}{dC_{at_B}} \approx \frac{E_p}{2}\left(R_{el}\left(\frac{N_{val_B}}{N_{val_{Si}}} - 1\right) + 1 - \frac{V_{at_B}}{V_{at_{Si}}}\right), \qquad (6)$$

where $V_{at_{Si}}$ and V_{at_B} are the volumes of Si and B atoms derived from their covalent radii (84 and 111 pm, respectively), $N_{val_{Si}}$ and N_{val_B} are the valences of Si and electrically activated B atoms (4 and 3, respectively, assuming that no electrically active B atoms are passivated by H atoms) and R_{el} is the fraction of B that is electrically active (see Appendix).

Table II also gives values of dE_p/dC_B calculated on the assumption that R_{el} takes a representative value for 1% B doping of ~10%,[23,24] that the covalent radius of a C atom is 70 pm and that the average valence of *a*-Si:C:H is 4. The calculated dE_p/dC_B values reflect the lower rate of increase in plasmon peak energy for *a*-Si:C:H compared to *a*-Si:H, resulting primarily from the smaller average radius of the C-containing compound. Nevertheless, *a*-Si:H is a complex system and many approximations and assumption have been made in this calculation. In particular a larger covalent radius may be appropriate in *a*-Si:H for both Si and B (Ref. 21) and a value for the valence of Si atoms of ~2.4 has been reported for *a*-Si.[25]

The plasmon peak width ΔE_p is inversely proportional to the plasmon relaxation time (see Eq. (2)). The measured values of ΔE_p shown in Fig. 9 increase with decreasing B concentration, taking values between 4.7 and 5.4 eV, compared to a value of 3.7 eV calculated for crystalline Si for a low collection angle.[13] The 10 mrad collection angle used in the present study may contribute to the broadening of the plasmon peak. The number of oscillations that occur during the plasmon relaxation time $E_p/(2\pi\Delta E_p)$ is 0.7 for crystalline Si.[13] In our samples, the lower number of oscillations (approximately 0.5-0.6) is attributed to the amorphous structure and the presence of hydrogen, which may act as a scattering centre and contribute to ionized impurity scattering.[26]

We find that the relaxation time increases with increasing B concentration. Although this trend is not understood, it suggests that B atoms introduced by doping do not act as strong scattering centres. It has been reported that a direct effect of plasmon scattering is a reduction in mobility[27] (in the doping range 5×10^{17} to 5×10^{19} cm^{-3}, which corresponds to the typical B concentration measured in our solar cells). The lower plasmon width in the B-doped layer or in *a*-Si:H compared to *a*-Si:C:H may therefore be related to different mobilities.

CONCLUSIONS

We have demonstrated that core-loss EELS can be used to measure B concentrations in *p*-doped layers in *a*-Si:H and *a*-Si:C:H *n-i-p* solar cells. A fitting procedure is used to separate the B K edge contribution from the Si fine structure. B concentrations as low as 1 at. % are measured using EELS and compared with SIMS measurements made on the same samples. Low-loss EELS is used to measure changes in volume plasmon peak energy and peak width with B concentration. The plasmon energy is observed to increase by 0.1 eV with increasing B concentration, while the peak width is observed to decrease by ~0.2 eV. Possible explanations for these changes are discussed.

ACKNOWLEDGMENTS

The authors are grateful to J.-P. Barnes and M. Veillerot for the SIMS measurements and B. E. Kardynal for a critical reading of the manuscript. This work has been supported financially by the EU (Silicon-Light project EU FP-7 Energy 2009-241477).

APPENDIX: DERIVATION OF EQUATION (6)

The derivation of Eq. (6) is as follows:

If $V_{at_{Si}}$ and V_{at_B} are the covalent volumes of Si and B atoms,
$N_{at_{Si}}$ and N_{at_B} are the numbers of atoms of Si and B contained in volume V_0,
N_{el} is the number of electrically active B atoms in volume V_0,
$N_{val_{Si}}$ and $N_{val_{Bi}}$ are the valences of Si and electrically active B atoms (with no electrically active B atoms passivated by H atoms),
$C_{at_B} = \frac{N_{at_B}}{N_{at_{Si}}}$ is the atomic concentration of B,
$C_{el} = \frac{N_{el}}{N_{at_{Si}}}$ is the concentration of electrically active B,
$R_{el} = \frac{N_{el}}{N_{at_B}} = \frac{C_{el}}{C_{at_B}}$ is the ratio of electrically active to total B, which is assumed to be independent of B concentration and

$$V_0 = V_{at_{Si}}N_{at_{Si}} + V_{at_B}N_{at_B} = N_{at_{Si}}(V_{at_{Si}} + C_{at_B}V_{at_B}).$$

Then for undoped *a*-Si:H the electron density

$$n_{e_{Si}} = \frac{N_{val_{Si}}N_{at_{Si}}}{V_0} = \frac{N_{val_{Si}}}{V_{at_{Si}}} \approx \frac{4}{\frac{4}{3}\pi(117\,\text{pm})} \approx 610^{23}\ \text{e}^-/\text{cm}^{-3},$$

and for B-doped *a*-Si:H the electron density

$$
\begin{aligned}
n_e &= \frac{N_{val_{Si}}(N_{at_{Si}} + (N_{at_B} - N_{el})) + N_{val_B}N_{el}}{V_0} \\
&= \frac{N_{at_{Si}}(N_{val_{Si}}(1 + C_{at_B} - C_{el}) + N_{val_B}C_{el})}{N_{at_{Si}}(V_{at_{Si}} + C_{at_B}V_{at_B})} \\
&= \frac{N_{val_{Si}}}{V_{at_{Si}}} \frac{1 + C_{at_B} + C_{el-act_B}\left(\frac{N_{val_B}}{N_{val_{Si}}} - 1\right)}{1 + C_{at_B}\frac{V_{at_B}}{V_{at_{Si}}}} \\
&= \mathrm{n}_{e_{Si}} \frac{1 + C_{at_B} + C_{el-act_B}\left(\frac{N_{val_B}}{N_{val_{Si}}} - 1\right)}{1 + C_{at_B}\frac{V_{at_B}}{V_{at_{Si}}}} \\
&= \mathrm{n}_{e_{Si}} \frac{1 + C_{at_B}\left(R_{el}\left(\frac{N_{val_B}}{N_{val_{Si}}} - 1\right) + 1\right)}{1 + C_{at_B}\frac{V_{at_B}}{V_{at_{Si}}}}.
\end{aligned}
$$

It follows that

$$
\frac{dn_e}{dC_{at_B}} = n_{e_{Si}}\left(\frac{R_{el}\left(\frac{N_{val_B}}{N_{val_{Si}}} - 1\right) + 1}{1 + C_{at_B}\frac{V_{at_B}}{V_{at_{Si}}}} - \frac{\frac{V_{at_B}}{V_{at_{Si}}}\left(1 + C_{at_B}\left(R_{el}\left(\frac{N_{val_B}}{N_{val_{Si}}} - 1\right) + 1\right)\right)}{\left(1 + C_{at_B}\frac{V_{at_B}}{V_{at_{Si}}}\right)^2}\right),
$$

$$
n_{e_{Si}} = \left(R_{el}\left(\frac{N_{val_B}}{N_{val_{Si}}} - 1\right) + 1 - \frac{V_{at_B}}{V_{at_{Si}}}\right).
$$

The dependence of plasmon energy on B concentration is then obtained by making use of the expression derived from Eq. (3)

$$
\frac{dE_p}{dn_e} = \frac{E_p}{2\mathrm{n}_e},
$$

where we assume that $n_e \approx n_{e_{Si}}$ i.e.,

$$
\frac{dE_p}{dC_{at_B}} = \frac{dE_p}{dn_e}\frac{dn_e}{dC_{at_B}} \approx \frac{E_p}{2}\left(R_{el}\left(\frac{N_{val_B}}{N_{val_{Si}}} - 1\right) + 1 - \frac{V_{at_B}}{V_{at_{Si}}}\right).
$$

[1]P. Couty, M. Duchamp, K. Söderström, A. Kovacs, R. E. Dunin-Borkowski, L. Sansonnens, Y. Ziegler, H. Ossenbrink, A. Jager-Waldau, and P. Helm, in *Transmission Electron Microscopy of Amorphous Tandem Thin-Film Silicon Modules Produced by A Roll-to-Roll Process on Plastic Foil: Proceedings of the 26th European Photovoltaic Solar Energy Conference and Exhibition*, Hamburg, Germany, 5-6 Sept. 2011, edited by EU PVSEC, p. 2395.

[2]B. B. Van Aken, M. Duchamp, C. B. Boothroyd, R. E. Dunin-Borkowski, and W. J. Soppe, J. Non-Cryst. Solids **358**, 2179 (2012).

[3]M. Aboy, L. Pelaz, P. Lopez, E. Bruno, and S. Mirabella, in *Carrier Mobility Degradation in Highly B-Doped Junctions: Proceedings of the Spanish Conference on Electron Device*, edited by A. G. Loureiro, N. S. Iglesias, N. A. A. Rodriguez, and E. C. Figueroa, (IEEE), Santiago de Compostella, Spain, 11-13 February, 2009, p. 34.

[4]B. Caussat, E. Scheid, B. De Mauduit, C. Dubois, G. Prudon, B. Gautier, and R. Berjoan, Thin Solid Films **446**, 218 (2004).

[5]U. Kroll, C. Bucher, S. Benagli, I. Schonbachler, J. Meier, A. Shah, J. Ballutaud, A. Howling, Ch. Hollenstein, A. Buchel, and M. Poppeller, Thin Solid Films **451**, 525 (2004).

[6]B. Lim, F. Rougieux, D. Macdonald, K. Bothe, and J. Schmidt, J. Appl. Phys. **108**, 103722 (2010).

[7]K. Bothe and J. Schmidt, J. Appl. Phys. **99**, 013701 (2006).

[8]M. Duchamp, C. B. Boothroyd, A. Kovacs, S. Kadkhodazadeh, T. Kasama, M. S. Moreno, B. B. Van Aken, J. P. Barnes, M. Veillerot, S. B. Newcomb, and R. E. Dunin-Borkowski, J. Phys.: Conf. Ser. **326**, 012052 (2011).

[9]Y. Zhu, R. Egerton, and M. Malac, Ultramicroscopy **87**, 135 (2001).

[10]C. B. Boothroyd, K. Sato, and K. Yamada, in *The Detection of 0.5 at. % Boron in Ni2Al Using Parallel Energy-Loss Spectroscopy: Proceedings of the XII International Congress on Electron Microscopy*, edited by L. D. Peachey and D. B. Williams, Seattle, Washington, 12-18 August 1990, (San Francisco Press, San Francisco, 1990), p. 80.

[11]R. F. Egerton, Microsc. Microanal. Microstruct. **2**, 203 (1991).

[12]K. Asayama, N. Hashikawa, K. Kajiwara, T. Yaguchi, M. Konno, and H. Mori, Appl. Phys. Express **1**, 074001 (2008).

[13]R. F. Egerton, *Electron Energy-Loss Spectroscopy in the Electron Microscope* (Plenum Press, New-York, 1986).

[14]B. B. Van Aken, C. Devilee, M. Dörenkämper, M. Geusebroek, M. C. Heijna, J. Löffler, and W. J. Soppe, J. Non-Cryst. Solids **354**, 2392 (2008).

[15]R. D. Leapman, P. Rez, and D. F. Mayers, J. Chem. Phys. **72**, 1232 (1980).

[16]T. Williams, C. Kelley, and many others, Gnuplot 4.4: an interactive plotting program, 2010, see http://gnuplot.sourceforge.net.

[17]B. Poe, F. Seifert, T. Sharp, and Z. Wu, Phys. Chem. Miner. **24**, 477 (1997).

[18]V. I. Ivashchenko, P. E. A. Turchi, V. I. Shevchenko, L. A. Ivashchenko, and G. V. Rusakov, J. Phys. Condens. Matter **15**, 4119 (2003).

[19]M. Moreno, K. Jorissen, and J. Rehr, Micron **38**, 1 (2007).

[20]C. Dubois, G. Prudon, B. Gautier, and J.-C. Dupuy, Appl. Surf. Sci. **255**, 1377 (2008).

[21]J. M. Holender and G. J. Morgan, Model. Simul. Mater. Sci. **2**, 1 (1994).

[22]D. B. Williams and J. W. Edington, J. Microsc. **108**, 113 (1976).

[23]M. Stutzmann, Philos. Mag. B **53**, L15 (1986).

[24]M. Stutzmann, D. K. Biegelsen, and R. A. Street, Phys. Rev. B **35**, 5666 (1987).

[25]S. Elliott, Adv. Phys. **38**, 1 (1989).

[26]T. D. Veal, G. R. Bell, and C. F. McConville, J. Vac. Sci. Technol. B **20**, 1766 (2002).

[27]H. Kosina and G. Kaiblinger-Grujin, Solid State Electron. **42**, 331 (1998).